Journal of Physics:
Condensed Matter

PAPER • **OPEN ACCESS**

Visible proton Bragg curve imaging by colour centre photoluminescence in radiation detectors based on lithium fluoride films on silica

To cite this article: R M Montereali *et al* 2024 *J. Phys.: Condens. Matter* **36** 215703

OPEN ACCESS
IOP Publishing
Journal of Physics: Condensed Matter
J. Phys.: Condens. Matter **36** (2024) 215703 (7pp)
https://doi.org/10.1088/1361-648X/ad2a08

Visible proton Bragg curve imaging by colour centre photoluminescence in radiation detectors based on lithium fluoride films on silica

R M Montereali[1,*], V Nigro[1], M Piccinini[1], M A Vincenti[1], P Nenzi[1], C Ronsivalle[1] and E Nichelatti[2]

[1] ENEA C.R. Frascati, Fusion and Technologies for Nuclear Safety and Security Department, Via E. Fermi 45, 00044 Frascati (Rome), Italy
[2] ENEA C.R. Casaccia, Fusion and Technologies for Nuclear Safety and Security Department, Via Anguillarese 301, 00123 S. Maria di Galeria (Rome), Italy

E-mail: rosa.montereali@enea.it

Received 30 October 2023, revised 30 January 2024
Accepted for publication 16 February 2024
Published 27 February 2024

Abstract

Passive solid-state radiation detectors, based on the visible photoluminescence (PL) of radiation-induced colour centres in optically transparent lithium fluoride (LiF), polycrystalline thin films are under investigation for proton beam advanced diagnostics. After proton exposure, the latent images stored in LiF as local formations of stable F_2 and F_3^+ aggregate defects, are directly read with a fluorescence microscope under illumination in the blue spectral range. Adopting a suitable irradiation geometry, the energy density that protons deposit in the material can be recorded as a spatial distribution of these light-emitting defects, from which a luminous replica of the proton Bragg curve can be thereafter extracted and analysed to reconstruct the proton beam energy spectrum. Their peculiar properties, such as wide dynamic range and linearity of the spectrally-integrated PL response vs. dose, make the investigation of two-dimensional LiF film radiation detectors grown on several types of substrate highly attractive. Here, the case of a LiF thin film thermally evaporated on a silica substrate, irradiated at grazing incidence with a 35 MeV proton beam, is investigated and reported for the first time. A comparison of the measured photoluminescent Bragg curve with Monte Carlo simulations demonstrates that the Bragg peak in the film is located at the very same position that would be expected in the underlying silica substrate rather than in LiF. The film packing density is shown not to have a significant effect on the peak depth, while even small nonzero grazing angle of the impinging proton beam is able to significantly modify the shape of the Bragg curve. These findings are ascribed to the effects of multiple Coulomb scattering in both the film and the substrate and are interesting for proton beam diagnostics and dosimetry.

Keywords: photoluminescence, colour centres, proton Bragg peak, thin films, lithium fluoride

* Author to whom any correspondence should be addressed.

1. Introduction

Passive solid state radiation detectors based on photoluminescence (PL) of point defects in dielectrics [1–4] (crystals, glasses and films) are widely utilized for imaging and dosimetry and should feature high spatial resolution, long-term stability against fading, non-destructive reading capability, as well as optical transparency at the emission and excitation wavelengths. Due to the excellent optical and thermal properties of some laser-active radiation-induced colour centres (CCs) in lithium fluoride (LiF) [5], novel radiation detectors based on this material were proposed for the imaging of soft x-rays [6] in the form of optically transparent thin films [7], exploiting the visible PL of F_2 and F_3^+ aggregate CCs that are created by the irradiation. These intrinsic defects, consisting of two electrons bonded to two and three close anion vacancies, respectively, are stable at room temperature (RT) [5]. Their broad PL emission bands, located at ∼670 and ∼530 nm, respectively [8], are simultaneously excited in their almost overlapping absorption bands peaked at ∼450 nm [9], known as M band [8]. Under blue-light illumination, fluorescence microscopy is used for reading the spectrally-integrated visible PL emission of the x-ray induced F_2 and F_3^+ CCs locally created in the LiF matrix, whose concentration is point-by-point proportional to the energy deposited in the irradiated layer. The RT stability of F_2 and F_3^+ CCs in LiF, even in daylight, makes these solid state radiation detectors easy to handle; moreover, no development process is needed after irradiation. Their use in x-ray imaging at nanoscale [10] has been successfully extended to higher photon energies in different conditions and configurations, both in the form of crystals [11] and thin films [12]. A very high intrinsic spatial resolution is assured by the sub-nanometric dimensions of the fluorescent defects [13], practically limited only by the optical microscope and used technique [14].

In the last years, radiation detectors based on the visible PL of CCs in LiF crystals and thin films have been gaining an increasing attention for proton beam advanced diagnostics [15–18] at high accumulated doses. Exploiting the low thickness of LiF thin films, transversal dose mapping of low-energy proton beams was demonstrated [16]. Although use in dosimetry of PL from F_2 and F_3^+ CCs induced in LiF by radiation is not a new idea, as it was initially proposed for doped LiF pellets and pure LiF crystals at high doses [19, 20], only recently it was successfully tested at therapeutic doses with clinical X [21] and gamma rays [22]. LiF tissue equivalence is essential for meaningful applications in clinical dosimetry for radiotherapy, including protons at doses below 50 Gy [23, 24]. Recently, nominally pure LiF crystals were used as fluorescent nuclear track detectors of energetic charged particles [25, 26], mainly alpha and heavier ions. In the case of charged particles, the typical energy-loss curve vs. penetration depth in matter is known as the Bragg curve and features a maximum, called the Bragg peak, approximately located at the end of their path [27]. The formation of this peak is due to the inverse proportionality of the energy transferred in electromagnetic interactions to the proton velocity—indeed, the protons lose more and more energy per path length as they slow down. The depth of the Bragg peak depends on the composition of the irradiated material, it is inversely proportional to its density [28], and increases almost quadratically with the incoming proton energy E. A similar dependence on E holds for the proton maximum penetration, known as range R_B, which is approximately described by the well-known Bragg–Kleeman rule

$$R_B = \alpha E^p$$

where the two coefficients α and p were estimated for LiF bulk as ∼9.237 μm MeV^{p-1} and ∼1.797 [29], respectively, according to Monte Carlo simulations performed in Stopping and Range of Ions in Matter software [28].

A precise measurement of the proton energy corresponding to the Bragg peak is a desirable and useful beam diagnostic outcome. It was found that, by adopting a suitable grazing-incidence irradiation geometry, the energy density that protons deposit in LiF crystals can be recorded as a two-dimensional (2D) spatial distribution of light-emitting F_2 and F_3^+ defects, from which a luminous replica of the full proton Bragg curve can be thereafter extracted and analysed. This approach has been utilized to characterize the beam of the intensity modulated proton linear accelerator for radiotherapy linac during its commissioning. This radiofrequency pulsed linear accelerator is being developed at ENEA C.R. Frascati for proton-therapy purposes [30]. For the characterisations, LiF crystals were used to estimate the energy spectrum of the beam by imaging and fitting entire Bragg curves in a wide range of doses and energies from 3 up to 55 MeV, even in the case of multi-energetic beams [29]. It was experimentally found that the visible PL intensity of F_2 and F_3^+ CCs is linear with absorbed doses up to ∼10^5–10^6 Gy, with a wide dynamic range which reaches ∼114 dB in proton-irradiated LiF crystals, where the Bragg curve was fully reconstructed for a 35 MeV proton beam and an entrance dose of 50 Gy [23]. At this energy, a value for R_B of 5.49 mm is derived for a proton beam irradiating a homogeneous bulk LiF of density $\rho = 2.635$ g cm^{-3}.

Recently, we have been investigating the feasibility of extending this approach to LiF thin films deposited on silicon substrates by thermal evaporation [31, 32] with the aim of understanding the role and the effects of the substrate on how the recorded Bragg curves are shaped. In this work, the case of a polycrystalline LiF thin film deposited on a fused silica substrate by thermal evaporation and irradiated at grazing incidence with a proton beam of nominal energy 35 MeV is presented for the first time.

2. Materials and methods

An optically transparent LiF film, of thickness $t \sim 1.8$ μm, was grown by thermal evaporation at the edge of a circular fused silica (Suprasil®) substrate, 1 mm thick and diameter 20 mm, constantly kept at a temperature of 300 °C during deposition [33], which was performed in a vacuum chamber at a pressure below 1 mPa at ENEA C.R. Frascati with a controlled deposition rate of 1 nm s^{-1}.

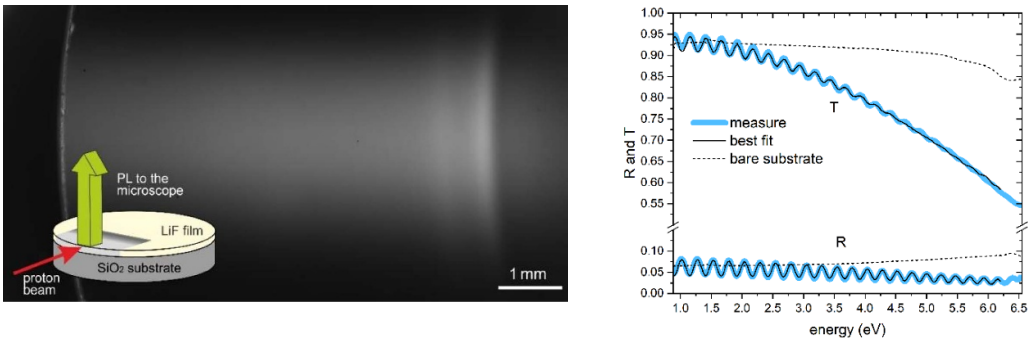

(a) (b)

Figure 1. (a) Fluorescence image of the top surface of the LiF film grown at the edge of a circular silica substrate, irradiated with a nominal 35 MeV proton beam (scale bar 1 mm). Inset: scheme of the proton irradiation geometry for the LiF film and PL collection geometry. (b) Direct transmittance and absolute specular reflectance spectra of the same LiF film, ∼1.8 μm thick, thermally evaporated on the silica substrate kept at a constant temperature of 300 °C during the deposition, and their best-fit, see the text for details. For comparison, the measured optical spectra of the bare silica substrate are also shown.

The direct transmittance and specular reflectance optical spectra were measured using a Perkin Elmer Lambda 1050 spectrophotometer. These photometric spectra were analysed and best fitted with a Matlab [34] homemade program using a thin-film theoretical model that includes several parameters: complex refractive index spectral dispersion, gradient of the refractive index along the growth axis, film thickness, and roughness [35].

A PARK System atomic force microscopy (AFM), model XE-150, operating in air in non-contact mode, was used to perform the morphological analysis of the LiF film surface.

The proton irradiation was performed in air at the nominal energy of 35 MeV. The beam direction was set at grazing incidence to ensure proton penetration and stopping inside the sample, as sketched in the inset of figure 1(a). The duration of the beam pulses was 2.5 μs full width half maximum (FWHM) at a typical repetition rate of 25 Hz; the average beam current was 20 μA. The irradiation dose in LiF at the LiF/air interface of the film (the entrance point of the beam) was 10^4 Gy.

After irradiation, the latent 2D fluorescence image of the accumulated CCs distributions generated and stored in the LiF film detector was acquired from the top face of the film by a fluorescence microscope Nikon Eclipse 80i, equipped with proper optically filtered Hg lamp and an Andor Neo s-CMOS camera, with an 11-bit dynamic range.

Energy deposition by protons in the LiF film was simulated using Monte Carlo FLUKA software (version 4–2.2) [36–38] equipped with the graphical user interface Flair (version 3.1–15) [39].

3. Results and discussion

Figure 1(a) shows the PL image of the LiF film thermally evaporated at the edge of the silica substrate after nominal 35 MeV proton irradiation. In the inset of figure 1(a), the irradiation geometry is sketched. The circular shape of the substrate is well distinguished, on the left, due to light scattering at the film border on the unpolished silica edge. The white areas are the portions of the LiF film surface irradiated by the proton beam, whose transversal elliptical shape has dimensions of (5×1) mm^2 at a distance of 20 mm from the titanium exit window of the linac. At least two PL intensity maxima are clearly distinguished close to the end of the proton path in LiF.

The structural, morphological and optical properties of a polycrystalline LiF film grown on an amorphous substrate, like silica, are strongly influenced by the selected growth conditions [7, 33], among them the substrate temperature during the growth and the total film thickness. Figure 1(b) reports the direct transmittance and absolute specular reflectance of the same film, measured between 190 and 1200 nm before irradiation. The spectra of the bare silica substrate are also shown for comparison. By using a best-fit procedure with an ad hoc model [35], the main physical characteristics of the LiF layer could be estimated in a quantitative way. The refractive index and the extinction coefficient spectral dispersion curves at half thickness of the LiF film are shown in figures 2(a) and (b), respectively. In figure 2(a), the refractive index of bulk LiF is also reported as found in the literature [40]. Note that a reduced density of the layer can be ascribed to the polycrystalline nature of LiF thin films, which can be considered as aggregates of grains with air interstices. As a matter of fact, from the best fit procedure, a refractive index of (1.330 ± 0.005) at the wavelength of 633 nm was derived, a value lower than the bulk one, 1.391 [37], despite to the fact that a constant substrate temperature of 300 °C maintained during the growth process increases the mobility of film molecules and favours the formation of packed microcrystals. It should be considered that the total thickness of the film is quite high: an average thickness of (1822 ± 5) nm and an extinction coefficient of $(4.88 \pm 0.08) \times 10^{-3}$ were obtained, together with a surface root-mean-square roughness of (17.2 ± 0.3) nm. With the characterisation we also estimated a slight deviation of the film faces from parallelism of (1.5 ± 0.2)% and a slight linear inhomogeneity of the refractive index along the growth axis of (9.0 ± 0.9)%. Although a linear behaviour of such

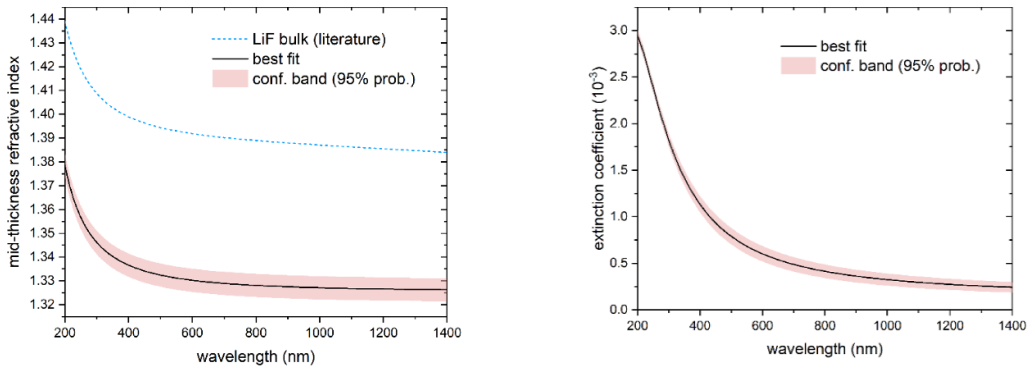

(a) (b)

Figure 2. Refractive index (a) and extinction coefficient (b) spectral dispersion curves (solid lines) at half thickness of the LiF film grown on the silica substrate as deduced from the best fit of the R and T optical spectra in figure 1(b). For comparison, in figure (a) the literature refractive index of bulk LiF [40] is also shown (dashed line).

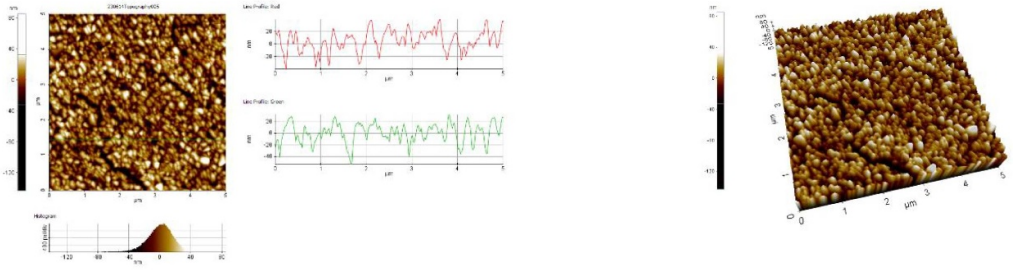

(a) (b)

Figure 3. 2D (a) and 3D (b) AFM images over an area of (5 × 5) μm^2 of the LiF film ∼1.8 μm thick, thermally-evaporated on the silica substrate kept at a constant temperature of 300 °C during the deposition.

inhomogeneity could be physically not fully correct, note that the best-fitting curves in figure 1(b) are practically coincident with the measured ones, therefore it can be considered a reliable approximation of the actual inhomogeneity. The packing-density of the film material, equal to the ratio of the actual LiF volume to the total film volume, was estimated from a comparison of the refractive index dispersion of the LiF film in figure 2(a) with that of LiF bulk [40]. By applying the effective medium theory [41] to a mixed medium composed of LiF hosting varying percentages of air inclusions, and comparing the resulting refractive index dispersions to that of the film, we were able to estimate the packing density of the polycrystalline material. At half-thickness it was estimated to be (84.5 ± 1.0)%. Due to the previously evaluated inhomogeneity along the growth axis, the packing density is lower at the LiF film-silica interface (69.5 ± 1.0)% and it raises to (99.5 ± 1.0)% at the LiF film-air interface.

In figures 3(a) and (b) the 2D and 3D AFM images over an area of (5 × 5) μm^2 of the LiF film thermally-evaporated on the silica substrate are shown. They demonstrate that the polycrystalline film is quite homogeneous. Moreover, the value of the root mean square roughness, measured along the red and green solid lines in figure 3(a), is about 16.3 nm, which is in good agreement with the value of 17.2 nm estimated from the spectrophotometric characterization.

Figure 4(a) shows the normalised PL intensity profile of the Bragg curve (solid line), as derived from the LiF film grown on silica after spatial integration on a selected region of interest of the PL image in figure 1(a) and background subtraction. It is compared with those measured in a LiF film grown on Si(100) (dashed line) and in a LiF crystal (dotted line) irradiated under the same conditions [31]. Their spatial alignment is performed by exploiting the peak of scattered light at the entrance border of impinging protons and, in the figure, the depth of the exposed sample edge is $d = 0$. It can be noticed that the peculiar convex shape of the curve recorded in the LiF film grown on silica is very similar to that of the film grown on the silicon substrate. This feature is ascribed to a slightly nonzero grazing incidence angle of the impinging proton beam during irradiation [31]. In both films, two maxima are evident towards the end of the Bragg curve and their distance is higher in the LiF film grown on silica with respect to silicon. Moreover, for both substrates, the Bragg peaks in the films are located at a significantly deeper position than that observed in the LiF crystal.

The low values of dose chosen for the irradiations ensured that the densities of the F_2 and F_3^+ CCs in LiF were linearly proportional to the absorbed energy at any point of their spatial distributions [15, 42]. In this way, we could exclude from our elaborations any density saturation effects. In these conditions,

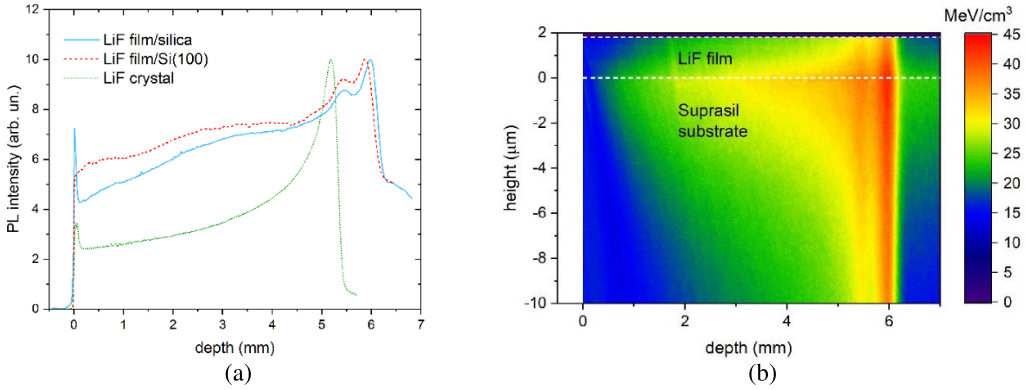

Figure 4. (a) Experimental PL intensity profile of Bragg curve extracted from the fluorescence image in figure 1(a) for the proton-irradiated LiF film grown on silica substrate (solid line), compared with those measured in the LiF film grown on Si(100) (dashed line) and in the LiF crystal (dotted line) (b) FLUKA simulation of the spatial distribution of deposited energy per proton within the LiF film with a mean packing density of 84.5% and within the top 10 μm of the silica substrate.

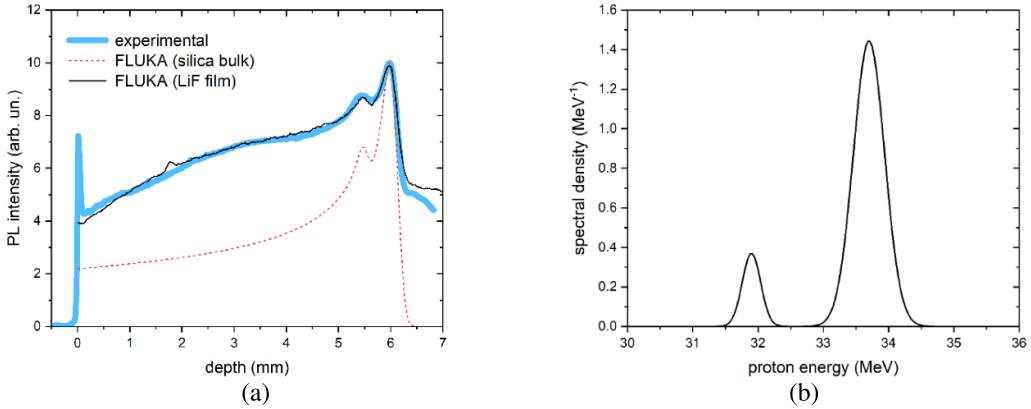

Figure 5. (a) Normalized simulated energy deposition profile in figure 4(b) within the film (black solid line), experimental PL intensity profile (blue thick solid line), normalized energy deposition profile in silica bulk (red dashed line) simulated with the same grazing angle and energy spectrum of the simulation of the actual thin film sample. (b) Proton-beam energy spectrum utilized for the FLUKA simulation of the LiF film on silica and of the silica bulk, see figure 4(a) and table 1.

the visible PL intensity is proportional point by point to the linear energy transfer (LET) curve. In the crystal, the PL intensity curve is a direct representation of the Bragg curve: the initial LET value is lower and almost constant at the entrance and raises to a maximum at the Bragg peak. This peak is quite broad, because the proton beam is not strictly monochromatic and two energy components are needed to reproduce it by the FLUKA code [31]. It was found that the electric-field phase in the last two active modules affects the energy distribution at the linac output. The presence of a second energy component is more evident in the LiF film PL profiles, were the two peaks are more clearly distinguished. In a homogeneous medium, the mean packing density value of 84.5% found for the film grown on silica causes the protons to have a longer range than in a LiF crystal, in agreement with the Bragg–Kleeman rule. Its value could quantitatively explain the observed differences in the depth of the main peak, which moves from ∼5.1 mm in the LiF crystal to ∼6.0 mm in the LiF film, as there is an accidental coincidence between the Bragg peak positions expected in the silica substrate and in a homogeneous LiF with this reduced density. However, this shift cannot be ascribed to a reduced density of the polycrystalline LiF layer, but is due to the presence of the thick silica substrate and to the limited thickness of the film, as detailed in the following. Only accurate Monte Carlo simulations, which take into account how multiple Coulomb scattering influence proton propagation in the layered structure constituted by the LiF thin film on the silica substrate, can provide a complete explanation of the observed behaviour and an accurate reconstruction of the full Bragg curve.

In this regard, a series of FLUKA simulations was conducted by incrementally adjusting specific parameters of the proton beam, including grazing angle and energy spectrum, aiming to replicate the experimental PL profile, as discussed later and shown in figure 5(a). Figure 4(b) reports the simulated spatial distribution of deposited energy density per proton within the film and the top 10 μm of the silica substrate. In this figure, two mutually close peaks are visible at the depths ∼5.4 and ∼6.0 mm.

They can be attributed to two energy components in the impinging proton beam, whose depths in the LiF film match those in the silica substrate, as figure 4(b) clearly shows. Such

Table 1. Parameters of the two energy-spectrum Gaussian components utilized for the FLUKA simulations of the LiF film thermally evaporated on silica and of the silica bulk in figure 5(a).

Energy component	Mean energy (MeV)	Standard dev.(keV)	Amount (%)
Main (film on silica)	33.7	240	87
Secondary (film on silica)	31.9	140	13

a coincidence is ascribed to the fact that the Bragg peaks in the LiF film are formed by protons that have travelled mainly through the underlying silica substrate.

This behaviour is confirmed by the comparison of the experimental PL depth profiles for the proton irradiated LiF film grown on silica substrate with the simulated ones, shown in figure 5(a). The calculated energy profiles demonstrate that the positions of the two Bragg peaks in the film match those expected in a silica bulk. This observation provides additional confirmation that protons contributing to energy deposition in the film predominantly traverse the substrate. On the other hand, protons entering the film at the depth $d = 0$ mostly leak from it due to multiple Coulomb scattering. Consequently, the substantial presence of protons from the silica substrate within the film can be attributed to the substrate significantly greater thickness compared to the LiF thin film. As a further confirmation of this fact, several FLUKA simulations performed at this proton energy demonstrated that the effect of the packing density of the polycrystalline film on the Bragg peak depth is negligible, contrary to the case of protons with energies below 5 MeV [43].

The best matching FLUKA simulation in figure 5(a) was run with a nonzero grazing angle $\theta = -0.84°$, which means that the proton beam is slightly obliquely impinging onto the film top surface; as already mentioned, this misalignment is essential to reproduce the convex shape of the PL profile in the depth range 0–5 μm [31]. Table 1 reports the parameters of the two Gaussian energy components, while the corresponding energy spectrum is shown in figure 5(b).

4. Conclusions

High spatial resolution solid-state passive LiF film radiation imaging detectors are under development for the advanced diagnostics and dose mapping of proton beams by non-destructive optical readout of visible PL from radiation-induced CCs in a fluorescence microscope. The PL signal intensities of aggregate F_2 and F_3^+ CCs in proton-irradiated LiF films are significantly lower than in LiF crystals, by at least one order of magnitude. The difference in PL signal intensities between proton-irradiated LiF films and LiF crystals stems from the proton beam depositing a significantly larger fraction of energy in the substrates than in the films, owing to their substantial difference in thickness. This fact notwithstanding, optically transparent thin LiF film detectors are able to locally store information about the proton beam intensity in a wide dynamic range across a large field of view (>1 cm^2). Despite their low thickness, the linear behaviour of the integrated visible PL intensity over at least three orders of magnitude of dose, makes them suitable for being employed as 2D solid-state dosimeters, especially at high proton doses. However, the complex proton-matter interaction requires accurate Monte Carlo simulations to correctly estimate the energy spectrum of the impinging protons in a layered structure constituted by a LiF film on a thick substrate.

Recently, we analysed Bragg curves generated by 35 MeV protons impinging at grazing incidence onto LiF films on Si(100) substrates, showing that the depth of the Bragg peak in the films coincide with the one that would be found in the substrate on which the film is deposited rather than in the film material. In the case of a silica substrate, reported here for the first time, a similar peak position coincidence between film and substrate has been detected and the distortion of the Bragg-curve observed by PL in a thermally evaporated LiF films has been ascribed to a small non-zero grazing-angle irradiation. These findings, being consequences of multiple Coulomb scattering both in the film and the substrate, could be explained by accurate FLUKA Monte Carlo simulations. At the investigated proton energy, the effect of the reduced packing density of the LiF layer, related to the polycrystalline nature of the film and on the selected substrate and growth conditions, has been found to be negligible.

The matching of the Bragg peak depths with those expected in the silica substrate and the possibility of visualizing these peaks in the latent fluorescence replicas of the Bragg curves is interesting in the development of versatile LiF film detectors for proton beam diagnostics and dosimetry, whose application can be tailored by suitable choice of substrates and growth conditions.

Data availability statement

All data that support the findings of this study are included within the article (and any supplementary files).

Acknowledgments

Research partially carried out within the TECHEA (Technologies for Health) Project, funded by ENEA, Italy, and the TOP-IMPLART (Oncological Therapy with Protons—Intensity Modulated Proton Linear Accelerator for RadioTherapy) project, funded by Regione Lazio, Italy. The authors are indebted with A Rufoloni for AFM measurements and L Picardi for fruitful discussions.

ORCID iDs

R M Montereali https://orcid.org/0000-0002-5540-3363
V Nigro https://orcid.org/0000-0003-0389-9982
M A Vincenti https://orcid.org/0000-0002-6229-4898

References

[1] Olko P 2010 Advantages and disadvantages of luminescence dosimetry *Radiat. Meas.* **45** 506
[2] Yukihara E G, McKeever S W S and Akselrod M S 2014 *Radiat. Meas.* **71** 15
[3] Yanagida T, Okada G, Kato T, Nakauchi D and Kawaguchi N 2022 A review and future of RPL dosimetry *Radiat. Meas.* **158** 106847
[4] Montereali R M, Nichelatti E, Nigro V, Piccinini M and Vincenti M A 2021 Radiophotoluminescence of color centers in lithium fluoride for novel radiation detectors in proton-beam diagnostics and clinical dosimetry *ECS J. Solid State Sci. Technol.* **10** 116001
[5] Basiev T T, Mirov S B and Osiko V V 1988 *IEEE J. Quantum Electron.* **24** 1052
[6] Baldacchini G, Bonfigli F, Faenov A, Flora F, Montereali R M, Pace A, Pikuz T and Reale L 2003 *J. Nanosci. Nanotechnol.* **3** 483
[7] Montereali R M 2002 *Handbook of Thin Film Materials* vol 3, ed H S Nalwa (Academic Press) ch 7, pp 399–431
[8] Nahum J and Wiegand D A 1967 *Phys. Rev.* **154** 817
[9] Voitovich A P, Kalinov V S and Stupak A P 2008 Luminescence excitation spectra and characteristics of luminescence centers with overlapping absorption bands *J. Appl. Spectrosc.* **75** 385
[10] Montereali R M, Bonfigli F, Nichelatti E, Piccinini M and Vincenti M A 2023 2.3 Luminescence of point defects in lithium fluoride thin layers for radiation imaging detectors at the nanoscale *Optical NanoSpectroscopy (Applications)* vol 3, eds A J Meixner, M Fleischer, D P Kern, E Sheremet and N McMillan (De Gruyter) pp 69–96
[11] Pikuz T A *et al* 2013 *Appl. Opt.* **52** 509
[12] Kurobori T and Matoba A 2014 *Jpn. J. Appl. Phys.* **53** 02BD
[13] Sekatskii S K and Letokhov V S 1996 *Appl. Phys.* B **63** 525
[14] Ustione A *et al* 2006 *Jpn. J. Appl. Phys.* **45** 2116
[15] Piccinini M, Ambrosini F, Ampollini A, Picardi L, Ronsivalle C, Bonfigli F, Libera S, Nichelatti E, Vincenti M A and Montereali R M 2015 Photoluminescence of radiation-induced color centers in lithium fluoride thin films for advanced diagnostics of proton beams *Appl. Phys. Lett.* **106** 261108
[16] Piccinini M, Nichelatti E, Ampollini A, Picardi L, Ronsivalle C, Bonfigli F, Libera S, Vincenti M A and Montereali R M 2017 *Eur. Phys. Lett.* **117** 37004
[17] Nichelatti E, Piccinini M, Ampollini A, Picardi L, Ronsivalle C, Bonfigli F, Vincenti M A and Montereali R M 2017 Bragg-curve imaging of 7 MeV protons in a lithium fluoride crystal by fluorescence microscopy of colour centres *Eur. Phys. Lett.* **120** 56003
[18] Picardi L *et al* 2020 Beam commissioning of the 35 MeV section in an intensity modulated proton linear accelerator for proton therapy *Phys. Rev. Accel. Beams* **23** 020102
[19] Levita M, Schlesinger T and Friedland S S 1976 LiF dosimetry based on radiophotoluminescence (RPL) *IEEE Trans. Nucl. Sci.* **23** 667
[20] Miller S D and Endres G W R 1990 *Radiat. Meas.* **33** 59
[21] Villarreal-Barajas J E, Piccinini M, Vincenti M A, Bonfigli F, Khan R and Montereali R M 2015 *IOP Conf. Ser.: Mater. Sci. Eng.* **80** 012020
[22] Piccinini M, Nichelatti E, Pimpinella M, De Coste V and Montereali R M 2022 Dose response of visible color center radiophotoluminescence in lithium fluoride crystals irradiated with a reference ^{60}Co gamma beam in the 1–20 Gy dose range *Radiat. Meas.* **151** 106705
[23] Piccinini M *et al* 2020 Dose response and Bragg curve reconstruction by radiophotoluminescence of color centers in lithium fluoride crystals irradiated with 35 MeV proton beams from 0.5 to 50 Gy *Radiat. Meas.* **133** 106275
[24] Piccinini M, Nichelatti E, Vincenti M A, Nigro V, Ronsivalle C, Ampollini A, Nenzi P, Bazzano G, Trinca E and Montereali R M 2023 Dynamic range and dose linearity of the radiophotoluminescence intensity in lithium fluoride crystals irradiated with 2.3 and 26 MeV protons *J. Lumin.* **259** 119833
[25] Bilski P and Marczewska B 2017 Fluorescent detection of single tracks of alpha particles using lithium fluoride crystals *Nucl. Instrum. Methods Phys. Res.* B **392** 41
[26] Bilski P, Marczewska B, Gieszczyk W, Kłosowski M, Naruszewicz M, Zhydachevskyy Y, Sankowska M and Kodaira S 2019 Fluorescent imaging of heavy charged particle tracks with LiF single crystals *J. Lumin.* **213** 82
[27] Knoll G F 2010 *Radiation Detection and Measurement* 4th edn (Wiley)
[28] Ziegler J F, Ziegler M D and Biersack J P 2010 *Nucl. Instrum. Methods Phys. Res.* B **268** 1818
[29] Nichelatti E, Ronsivalle C, Piccinini M, Picardi L and Montereali R M 2019 An analytical approximation of proton Bragg curves in lithium fluoride for beam energy distribution analysis *Nucl. Instrum. Methods Phys. Res.* B **446** 29
[30] Ronsivalle C, Picardi L, Ampollini A, Bazzano G, Marracino F, Nenzi P, Snels C, Surrenti V, Vadrucci M and Ambrosini F 2015 *Eur. Phys. Lett.* **111** 14002
[31] Nichelatti E, Nigro V, Piccinini M, Vincenti M A, Ampollini A, Picardi L, Ronsivalle C and Montereali R M 2022 Photoluminescent Bragg curves in lithium fluoride thin films on silicon substrates irradiated with a 35 MeV proton beam *J. Appl. Phys.* **132** 014501
[32] Montereali R M, Nichelatti E, Nigro V, Picardi L, Piccinini M, Ampollini A, Libera S, Ronsivalle C and Vincenti M A 2023 Proton Bragg peak imaging by colour centre radiophotoluminescence in lithium fluoride thin film radiation detectors on silicon *J. Mater. Sci., Mater. Electron.* **34** 377
[33] Leoncini M *et al* 2019 *Opt. Mater.* **88** 580
[34] The Mathworks, Inc. MathWorks MATLAB, V. 7.10.0 (R2010a) 2010 (The MathWorks Inc) (available at: www.mathworks.com)
[35] Montecchi M, Montereali R M and Nichelatti E 2001 *Thin Solid Films* **396** 264 2002 *Thin Solid Films* **402** 311
[36] Ahdida C *et al* 2022 New capabilities of the FLUKA multi-purpose code *Front. Phys.* **9** 788253
[37] CERN (available at: https://fluka.cern) (Accessed October 2023)
[38] Battistoni G *et al* 2015 Overview of the FLUKA code *Ann. Nucl. Energy* **82** 10
[39] Vlachoudis V 2009 FLAIR: a powerful but user friendly graphical interface for FLUKA *Proc. Int. Conf. on Mathematics, Computational Methods & Reactor Physics (M&C 2009) (Saratoga Springs, New York)*
[40] Palik E D 1985 *Handbook of Optical Constants of Solids* vol 1 (Academic) p 675
[41] Niklasson G A, Granqvist C G and Hunderi O 1981 Effective medium models for the optical properties of inhomogeneous materials *Appl. Opt.* **20** 26–30
[42] Montereali R M *et al* 2022 *J. Phys.: Conf. Ser.* **2298** 012001
[43] Montereali R M, Nigro V, Piccinini M, Vincenti M A, Ampollini A, Nenzi P, Ronsivalle C and Nichelatti E 2023 Bragg curve detection of low-energy protons by radiophotoluminescence imaging in lithium fluoride thin films *Sensors* **23** 4779